Green Chemistry

Cutting-edge research for a greener sustainable future

Accepted Manuscript

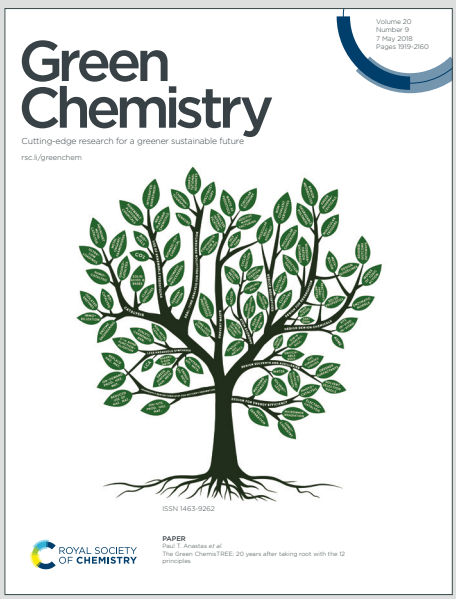

ROYAL SOCIETY OF CHEMISTRY

rsc.li/greenchem

View Article Online
DOI: 10.1039/C9GC01726G

One-pot Synthesized Core/Shell Structured Zeolite@Copper Catalysts for Selective Hydrogenation of Ethylene Carbonate to Methanol and Ethylene Glycol

Yu Ding, Jingxia Tian, Wei Chen, Yejun Guan, Hao Xu, Xiaohong Li,* Haihong Wu,* and Peng Wu*

Corresponding Address:

Shanghai Key Laboratory of Green Chemistry and Chemical Processes, School of Chemistry and Molecular Engineering, East China Normal University, North Zhongshan Rd. 3663, Shanghai 200062, PR China

Tel: *+86-21-6223-2292*

Fax: *+86-21-6223-2292*

E-mail address: pwu@chem.ecnu.edu.cn (P. Wu); *hhwu@chem.ecnu.edu.cn* (H. Wu) ; *xhli@chem.ecnu.edu.cn* (X. Li).

View Article Online
DOI: 10.1039/C9GC01726G

The copper-based catalysts, with highly dispersed and stabilized Cu nanoparticles, intensified mass transfer and well-balanced Cu^0/Cu^+ ratio at low Cu loadings, are highly desirable for the selective hydrogenation of ethylene carbonate to ethylene glycol and methanol, an efficient indirect route of CO_2 utilization. A hierarchically core/shell-structured Silicalite-1@Cu composite was developed via base-assisted chemoselective host-guest interaction between the silicon species of MFI-type Silicalite-1 and external Cu salt source. In-situ generated mesoporosity and strong Cu-silicate interaction made the uniform Cu NPs firmly immobilized and highly dispersed outside the core S-1 crystals. The S-1@Cu hybrid possessed the co-existing Cu^0/Cu^+ active species with a suitable ratio, and served as a highly active, selective and robust catalyst for selective ethylene carbonate hydrogenation, providing a lifetime >350 h together with >99% ethylene carbonate conversion, >99% ethylene glycol yield, and more importantly 93% methanol yield at a relatively low Cu loading of 21.4 wt.%.

View Article Online
DOI: 10.1039/C9GC01726G

Introduction

The increasing environmental concern of the elevated CO_2 level in atmosphere calls for innovative means to sequester and utilize it as a raw carbon source for producing chemicals and liquid fuels from the viewpoint of sustainable energy production.[1-4] A particularly attractive way of CO_2 utilization is to convert it to methanol (MeOH) by hydrogenation, a widely used fuel substitute and a versatile chemical intermediate on the basis of a "methanol economy" concept.[5-6] Direct catalytic hydrogenation of CO_2 to MeOH usually requires high temperature and pressure, due to the high activation energy for the cleavage of the C=O bonds in CO_2.[7-9] Therefore, the production of MeOH via direct hydrogenation route under mild condition is still a big challenge for both academia and industry.

Over the past years, the catalytic hydrogenation of organic carbonates has provided an alternative approach for the indirect transformation of CO_2 to MeOH, since the carbonates are synthesized easily from CO_2 and epoxides.[6,10-14] Ding and coworkers developed the hydrogenation of cyclic ethylene carbonate (EC) with a homogeneous PNP/Ru^{II} pincer complex under relatively mild conditions, affording two important bulk chemicals of MeOH and ethylene glycol (EG) at extremely high selectivity of 99%.[12] The homogeneous system would suffer the difficulties of catalyst-product separation in practical application. Li et al. reported the heterogeneous hydrogenation of EC using a copper chromite nanocatalyst which showed 60% and 93% selectivities towards MeOH and EG, respectively.[15] Nonetheless, the toxic chromium is unfriendly to human and environment. On the

View Article Online
DOI: 10.1039/C9GC01726G

other hand, the Cu-silica catalysts have been extensively studied in C=O hydrogenation. Liu and coworkers prepared an environmentally friendly Cu/SiO_2 catalyst with a Cu content high as 56 wt.% by precipitation-gel method, which owned remarkable activity and stability for EC hydrogenation in both batch-wise reactors and fixed-bed continuous flow reactors, showing the highest selectivity to MeOH (95%) and EG (97%).[16] Then, an efficient mesosilica-based Cu/HMS catalyst was developed via an ammonia evaporation method.[17] High yields of MeOH (74%) and EG (>99%) were then achieved along with complete conversion of EC (>99%) with a Cu loading of 44.6%. Very recently, we prepared a ternary Cu-Mg-Zr/SiO_2 catalyst using a co-precipitation method. Under optimal reaction conditions, this catalyst provided the MeOH selectivity above 80% at the complete conversion of EC, but requiring a Cu loading high as 60 wt.%.[18]

Although several excellent studies have been carried out with regards to the Cu/silica-based catalysts for the selective hydrogenation of EC to MeOH, relatively high hydrogen pressure or high Cu content was applied in most cases. In order to improve the MeOH selectivity, the second or the third component is usually indispensable for modulating the electronic properties of the Cu catalyst in a few cases. It is still challenging to achieve an efficient indirect conversion of CO_2 to MeOH with the monometallic Cu-based catalyst bearing a lower Cu content. In addition, earlier researches on understanding the active sites of copper catalysts indicated that the Cu^0 and Cu^+ species were both crucial to the catalytic ability of Cu-silica for EC hydrogenation. The Cu^+ sites may function as electrophilic or Lewis

View Article Online
DOI: 10.1039/C9GC01726G

acid sites to polarize the carbonyl groups via the electron lone pair in oxygen while the Cu^0 species adsorb H_2 dissociatively and facilitate the hydrogenation and/or hydrogenolysis reactions.[16,17,19-23] Hence, it is essential to fabricate the Cu-based catalysts in a precisely controlled manner with co-existing and stable Cu^0 and Cu^+ active species.

Herein, we developed a hydrothermal approach to synthesize core/shell S-1@Cu materials with Silicalite-1 as core and selectively immobilized Cu NPs outside the zeolite crystals, the chemistry of which is apparently different from conventional impregnation. The effects of zeolite topology, crystal size, roles of Cu^0 and Cu^+ species and the copper content on the catalytic performance for the selective hydrogenation of EC in a fixed-bed reactor were investigated in detail. Under the relatively mild conditions, the S-1@Cu catalyst with the optimal Cu loading of 21.4%, with the S-1 size of 210 nm, after reduction at 250 ºC, showed a high MeOH yield of (>93%) at almost complete conversion of EC (>99%) and 99% EG yield in a fixed-bed reactor, which is one of the best results with the Cu-based catalysts for the selective hydrogenation of EC reported in the literature up to now.

Experimental

Chemicals

Tetraethylorthosilicate (98%) and colloidal silica (30 wt.% in H_2O) were purchased from Sigma-Aldrich. Fumed SiO_2 (≥99%) was purchased from Qingdao Chemical Co., Ltd. Tetrapropylammonium hydroxide (25 wt.%) was purchased from TCI. Ammonium nitrate (≥99%) was purchased from Xilong Chemical Co., Ltd. Ethylene

View Article Online
DOI: 10.1039/C9GC01726G

carbonate (98%) was purchased from Aladdin. Tetrapropylammonium bromide (≥98%), ammonia solution (28 wt.%), $Cu(CH_3COO)_2 \cdot H_2O$ (≥98%), ethanol (≥99.7%), nitric acid (65 - 68 wt.%) and 1, 4-dioxane (≥99.5%) were purchased from Sinopharm Chemical Reagent Co., Ltd. and all of them were used as received. H_2, N_2 and 5%H_2/N_2 gases (99.999 vol. %) were supplied by Shanghai Pujiang Specialty Gases Co., Ltd.

Synthesis of Silicalite-1-210 (S-1-210)

Nanosized Silicalite-1 with an average size of 210 nm, denoted as S-1-210, was hydrothermally synthesized from the silica source of tetraethylorthosilicate (TEOS) using 25 wt.% tetrapropylammonium hydroxide (TPAOH) as oganic structure-directing agent (OSDA). The synthetic gel was prepared with molar compositions of 1.0 SiO_2 : 0.18 TPAOH: 18 H_2O. After stirring for 1 hour at room temperature, the gels were crystallized in Teflon-lined steel autoclaves at 120 ºC for 1 day and then at 170 ºC for 1 day. The S-1-210 products were collected by filtration followed by washing with distilled water several times, dried at 100 ºC overnight, and then calcined in air at 550 ºC for 6 h to remove the occluded organic template.

Synthesis of Core/shell S-1-210@Cu-y Catalyst via the Copper Silicate Precursors Coated on S-1-210 (S-1-210@$CuSiO_3$-y)

Firstly, S-1-210@$CuSiO_3$ was prepared through a one-step hydrothermal process. In a typical synthesis, $Cu(CH_3COO)_2 \cdot H_2O$ (0.2 - 0.4 g), 1.6 g NH_4NO_3 and 1.82 g $NH_3 \cdot H_2O$ (28%) were added under stirring to 100 g of distilled water. S-1-210 powder (0.3 g) was added to the above solution, and ultrasonic treatment was then

View Article Online
DOI: 10.1039/C9GC01726G

carried out for 0.5 h to disperse the pristine zeolite into a homogenized suspension. Then, the obtained mixture was transferred to a Teflon-lined stainless steel autoclave and heated at 150 ºC for 3 h. During this process, the Cu precursor interacted with the silicon species of S-1-210, inducing an epitaxial growth of layered copper silicate ($CuSiO_3$) phase on the S-1-210 crystal surface. After the autoclave was naturally cooled to room temperature, the solid products were collected by washing with deionized water and ethanol, and drying at 60 ºC overnight. Fianlly, they were calcined at 450 ºC in air for 4 h. The obtained composites were denoted as S-1-210@$CuSiO_3$-*y*, where *y* represents the weight percentage of Cu actually loaded. At last, the prepared core/shell S-1-210@$CuSiO_3$ was reduced under H_2 atmosphere (60 mL min^{-1}) at 150 - 450 ºC for 4 h with a heating rate of 2 ºC min^{-1}. The final obtained catalyst was denoted as S-1-210@Cu-*y*.

Synthesis of Other Zeolite@Cu Composites

For control experiment, the zeolite@Cu composites with different topologies such as the high silica beta (Beta-D) and MOR-D zeolites were also synthesized. The Si-rich Beta-D and MOR-D were obtained by a dealumination method (to see Experimental in the Supporting Information for details).[24] In addition, Silicalite-1 with larger sizes were also synthesized to prepare the S-1-x@Cu catalysts, where x represents the zeolite size. Silicalite-1 samples with larger sizes were hydrothermally synthesized by varying the gel composition, OSDA or silica source (to see the Supporting Information for details). The SEM investigation indicated that their crystals had the average sizes of 340 nm, 4800 nm and 30000 nm, which are denoted as S-1-340,

View Article Online
DOI: 10.1039/C9GC01726G

S-1-4800 and S-1-30000, respectively. The S-1-x@Cu and zeolite@Cu with different topologies containing an actual Cu content of about 22% was prepared using a similar method as that for S-1-210@Cu-21.4.

Characterization Methods

High resolution XRD data were recorded on a Bruker D8 Advance X-ray diffractometer with Cu-Kα radiation (λ = 1.5405 Å) at 35 kV and 25 mA. To improve accuracy, the sample was continuously rotated in a 0.5 mm glass capillary.

The contents of Si, Al and Cu were determined by inductively coupled plasma atomic emission spectrometry (ICP-AES) on a Thermo IRIS Intrepid II XSP atomic emission spectrometer after dissolving the samples in aqueous HF solution.

The textual properties of microporous/mesoporous hybrid materials were analyzed by nitrogen adsorption–desorption at 77 K on a BELSORP-MAX instrument after degassing at 573 K under vacuum for 6 h. The surface area was calculated with the Brunauer-Emmett-Teller (BET) method, while the total pore volume was accumulated from the adsorption capacity at P/P_0 = 0.99. The micropore and mesopore size distributions were calculated by the Saito-Foley (SF) and Barrer-Joyner-Halenda (BJH) methods, respectively.

Scanning electron microscopy (SEM) images were collected on a Hitachi S-4800 at 3 kV. The transmission electron microscopy (TEM) images were taken on a Tecnai G^2 F30 transmission electron microscope at 300 kV.

Fourier transform infrared (FTIR) spectra in the framework vibration region were collected on a Nicolet Nexus 670 FTIR spectrometer operated at a spectral resolution

View Article Online
DOI: 10.1039/C9GC01726G

of 2 cm^{-1} using KBr pellets of the solid samples.

The Pyridine-adsored FTIR spectra were collected on a Nicolet Nexus 670 FTIR spectrometer in transmittance mode at a spectral resolution of 2 cm^{-1}. The sample was pressed into a self-supported wafer with 4.8 mg cm^{-2} and set in a quartz cell sealed with CaF_2 windows. After reduced at 250 ºC for 4 h and evacuated at 250 ºC for 1 h, the wafer was exposed to a pyridine vapour at 25 ºC for 20 min. The adsorbed pyridine was evacuated successively from 25 to 150 ºC for 0.5 h.

The CO-adsored FTIR spectra were collected on a Nicolet Nexus 670 FTIR spectrometer in transmittance mode at a spectral resolution of 2 cm^{-1}. The sample was pressed into a self-supported wafer with 4.8 mg cm^{-2} and set in a quartz cell sealed with CaF_2 windows. After calcined at 450 ºC in N_2 for 1 h and reduced at 250 ºC for 4 h under H_2 atmosphere, the samples were exposed to 5% CO/Ar for 5 min. The spectra were collected after N_2 purging for 30 min. To investigate the amount of the surface Cu^+ species, the reduction temperatures on the S-1-210@$CuSiO_3$ catalysts were changed in the range of 150 to 450 ºC.

X-ray photoelectron spectroscopy (XPS) was performed with Al K_α ($h\nu$ = 1486.6 eV) radiation on a Thermo Scientific K-Alpha spectrometer. Charging effects were corrected by using the C 1s peak due to adventitious carbon with EB fixed at 284.6 eV. For the in situ experiments, the catalysts were reduced at from 150 to 450 ºC for 4 h in a flow of H_2 (60 mL min^{-1}). After cooling to room temperature, the pretreatment chamber was evacuated to 10^{-3} Pa, and then the reduced catalysts were transferred to the transfer chamber and further to the analytic chamber (10^{-9} Pa) for XPS

View Article Online
DOI: 10.1039/C9GC01726G

measurement without exposure to air.

The temperature-programmed desorption of ammonia (NH_3-TPD) was performed on Micrometrics tp-5080 equipment equipped with a thermal conductivity detector (TCD) detector. The TPD profile was recorded at a heating rate of 10 ºC min^{-1} from 100 to 900 ºC.

The carbon content of the used material was detected by thermogravimetric analysis (TG) in the temperature range of 25 - 800 ºC under an air flow.

The FTIR spectra of EC, MeOH and EG were collected on a Nicolet Nexus 670 FTIR spectrometer in absorbance mode at a spectral resolution of 2 cm^{-1} at 180 ºC against air background. The S-1-210@Cu-21.4 catalyst (20 mg) was mixed with 3 mg ethylene carbonate. Then the mixed sample was pressed into a self-supported wafer and was set in a quartz cell sealed with CaF_2 windows. Before the collection, the wafer was first purged for 10 min in a N_2 flow (30 mL min^{-1}) at room temperature. Then, the temperature program was started. When the temperature was increased to 180 ºC, the spectrum was collected in a N_2 atmosphere. The FTIR adsorption spectra of MeOH and EG were collected under similar experimental conditions as EC. A drop MeOH or EG was added to the S-1-210@Cu sample wafer, respectively. Then, the remaining operations were same as EG sample.

The FTIR spectra for the in-situ hydrogenation of EC was also collected on a Nicolet Nexus 670 FTIR spectrometer in absorbance mode at a spectral resolution of 2 cm^{-1}. Before the collection, the wafer of S-1-210@Cu with adsorbed EC was first purged for 10 min in a N_2 flow (30 mL min^{-1}) at room temperature. Then, the wafer was

View Article Online
DOI: 10.1039/C9GC01726G

heated to 180 °C with ramp rate of 10 °C min^{-1} and kept at this temperature. Afterwards, the wafer was exposed to 5% H_2/N_2 atmosphere. The spectra were collected after H_2/N_2 purging for 5 minutes.

Catalytic Hydrogenation of EC

The continuous flow EC hydrogenation reaction on different catalysts were performed using a fixed-bed reactor with 55 cm length and 12 mm inner diameter. The hydrogen flow rate was modulated using a mass flow controller and the pressure was controlled by a regulator valve. Firstly, 1.0 g of unreduced shaped catalysts (20 - 40 meshes) were loaded into the stainless steel tubular reactor with the thermocouple inserted into the catalyst bed. Before the reaction, the catalysts were reduced at 250 ºC for 4 h in a flow of H_2 (2 MPa, 60 mL min^{-1}). After cooling to the reaction temperature (180 ºC), 0.02 mL min^{-1} of 10 wt.% EC solution in 1,4-dioxane and 60 mL min^{-1} of H_2 with a system pressure of 4 MPa was adopted for a standard catalytic test. To investigate the influence of the surface Cu^0 and Cu^+ species to the reaction, the reduction temperatures on the S-1-210@$CuSiO_3$ catalysts were changed in the range of 150 to 450 ºC.

Alternatively, the hydrogenation of EC was also carried out in a batch reactor with a 100 mL-stainless steel autoclave at a stirring speed of 600 rpm. Firstly, the as-calcined catalysts were reduced at 250 ºC for 4 h in a flow of H_2 (60 mL min^{-1}). Then, the reduced catalyst (0.176 g) was transferred to the autoclave immediately without exposure and mixed with 10 mL of 10 wt.% EC in 1,4-dioxane. After fushing with H_2 five times, the autoclave was pressurized with H_2 pressure to 4 MPa, and then

View Article Online
DOI: 10.1039/C9GC01726G

heated to 180 ºC and kept steady during the reaction for 4 h. After the autoclave was completely cooled in an ice-water bath, the residual H_2 was released carefully

The products collected after 4 h of time-on-stream (TOS) or in a batch-wise reactor were analyzed offline using GC with an FID (TECHCOMP GC-7900 Plus, Tianmei Ltd. Co.). The response factor of each product, measured using corresponding authentic chemical, was used to calculate the conversion of EC and selectivities of EG and MeOH. The stability and lifetime of S-1-210@Cu-21.4 was evaluated continuously in the EC hydrogenation reaction and the reaction mixture was sampled with a time interval of 2 h.

Results and Discussion

Evolution of Active Copper Species and Morphology

The formation of the core/shell structure in S-1@Cu involves two steps as depicted in Scheme 1. Firstly, the needle-like copper silicate precursors were generated and coated on the outer surface of S-1 crystals through a base-assisted chemoselective interaction between zeolite Si species and the corresponding Cu salt source. This kind of host-guest chemical process takes place via the selective and partial dissolving of silica species off the S-1 crystals to form silicate anions, which then in-situ interact with the Cu cations in solution to form the layered copper phyllosilicates. As a result, a composite material with S-1 as core and copper silicate as shell are fabricated, which is similar to the chestnut shells. The hydrothermal reaction between SiO_2 and Cu^{2+} took place as follows: $2SiO_2 + 2Cu^{2+} + 4OH^- = Cu_2Si_2O_5(OH)_2 + H_2O$. The structure of copper phyllosilicate was stable even after

View Article Online
DOI: 10.1039/C9GC01726G

calcination.[23,25] The calcined sample S-1@$CuSiO_3$ was then subjected to H_2-reduction at an elevated temperature (150 - 450 ºC), converting the copper phyllosilicate precursors to the Cu_2O/Cu^0 species. The remaining SiO_2 matrices still maintained a needle-like morphology, whereas highly dispersed Cu NPs were immobilized therein, providing the S-1@Cu catalyst.

The active copper species of the S-1@Cu composites have been characterized by various techniques. The pristine S-1 (210 nm), S-1@$CuSiO_3$ and S-1@Cu showed well-resolved XRD patterns (Fig. 1), which are all characteristic of a typical MFI topology.[26] After the hydrothermal treatment of S-1 in a copper acetate solution and further calcination, the resultant S-1@$CuSiO_3$ showed a new diffraction at 2θ of 62.4º, which is assigned to the (362) plane of $Cu_2Si_2O_5(OH)_2$ (JCPDS No. 027-0188).[27] The H_2-reduced S-1@Cu exhibited new reflections at 2θ of 42.3º and 43.3º, which are indexed as crystalline Cu_2O (JCPDS No.05-0667) and Cu^0 (JCPDS No. 04-0836), respectively, indicating that the copper silicate phase was reduced to the Cu^+/Cu^0 species. The diffractions of Cu^0 or Cu^+ are rather weak in intensity, implying that the Cu species are highly dispersed on the support S-1 crystals. The FTIR spectroscopy was further employed to discriminate the Cu species. Two new shoulder bands appeared at 670 and 1025 cm^{-1} in S-1@$CuSiO_3$ in comparison to pristine S-1 (Fig. 2), which are ascribed to the frequencies of the δ_{OH} and ν_{SiO} modes of the Cu-O-Si bonds in the copper silicate formed.[27,28] The H_2-reduction vanished these two bands for S-1@Cu (Fig. 2c), implying copper silicate was transferred of to the Cu^+/Cu^0 species. The in-situ XPS spectra shown in Fig. 3A indicated the disappearance of the satellite

View Article Online
DOI: 10.1039/C9GC01726G

peak after reduction, which also confirmed that copper species were reduced to Cu^0 or/and Cu^+.[29,30] The peaks in Cu LMM were deconvoluted using Lorenz/Gaussian of 1/99.[18,30, 31-37] The peaks at 569.5 eV are assigned to Cu^0 species, while the peak at 571.5 eV is attributed to Cu^+ species. The Cu LMM Auger electron spectrum was measured to quantitatively discriminate the Cu^+ and Cu^0 species in S-1@Cu (Fig. 3B), which was in agreement with the former XRD observation. Thus, various characterizations consistently verified that the Cu species mainly existed as active Cu_2O and Cu^0 species in S-1@Cu.

The morphology and structure of the samples obtained at different stages were investigated by SEM and TEM images. The pristine S-1 crystals were of uniform nanosphere aggregations with a smooth surface (Fig. S1). After the hydrothermal treatment of S-1 in the cationic cuprammonia complex solution and further calcination, a core/shell-structured composite S-1@$CuSiO_3$ was as-fabricated, having a shell evenly covered by the needle-like nanorods with an average diameter of 4.8 nm, (Fig. 4a-c). Combined with the XRD and IR investigations, the nanorods were reasonably attributed to the $Cu_2Si_2O_5(OH)_2$ phase *in-situ* grown on the S-1 crystal surface.

S-1@Cu obtained by subsequent H_2-reduction still possessed a good core/shell structure, while the $Cu_2Si_2O_5(OH)_2$ precursors were decomposed and converted into the spherical Cu NPs and SiO_2 nanorods in shell (Fig. 4d-f and S2). The Cu NPs with 2 - 7 nm diameters were homogeneously dispersed on the SiO_2 nanorods derived from the Cu-Si precursors in shell. The N_2 adsorption-desorption isotherms of S-1 are of

View Article Online
DOI: 10.1039/C9GC01726G

typical type I of microporous materials, whereas those of S-1@Cu are of type IV (Fig. 5), implying that the latter is characteristic of microporous-mesoporous hybrid materials. After introducing Cu NPs into S-1, the specific surface area (SSA) slightly decreased from 364 $m^2 g^{-1}$ for S-1 to 335 $m^2 g^{-1}$ for S-1@Cu-21.4, meanwhile the external surface area (S_{ext}) remarkably increased to 117 $m^2 g^{-1}$ from 57 $m^2 g^{-1}$ and the mesopore volumes (V_{meso}) increased from 0.12 to 0.41 $cm^3 g^{-1}$ (Table 1). With a novel core/shell structure, confined space and improved transportation porosities, the S-1@Cu composites are expected to be promising catalysts for the selective hydrogenation of EC.

Effect of Zeolite Topology

The zeolite@Cu catalysts were employed to the EC hydrogenation for the selective production of MeOH and EG, an alternative route of CO_2 utilization as a renewable carbon source. Firstly, we studied the effect of zeolite topology on the MeOH selectivity. The Cu NPs were immobilized on other two representative silicates, e.g. *BEA and MOR using the similar method as that for S-1@Cu. The *BEA zeolite possessed three-dimensional mutually perpendicular 12-membered ring apertures and the MOR topology owned two pore channels of 12-membered ring and 8-membered ring along [001]. By screening the catalytic properties of Beta-D@Cu, MOR-D@Cu and S-1@Cu in EC hydrogenation, the MFI zeolite with 3D 10-ring (R) channels proved to be an optimal core or support for this target reaction. Among three zeolite@Cu catalysts with comparable Cu contents, S-1@Cu furnished the highest MeOH selectivity at almost complete EC conversion (Table S1), which is probably

View Article Online
DOI: 10.1039/C9GC01726G

contributed by the weak acidity and basicity properties of MFI structure as well as its proper interaction with the active metal.[16,27,38-40] The acid properties of different zeolite@Cu were investigated by FTIR spectroscopy. The stretching band of pyridinium ion at around 1540 and 1450 cm^{-1} were attributed to Brønsted (BAS) and Lewis (LAS) acid sites.[41] Fig. S3 shows the FTIR spectra after removing the physical adsorption of pyridine molecules. The amount of LAS on S-1@Cu was relatively smaller in comparison with Beta-D@Cu and MOR-D@Cu and almost no BAS was observed, which is surmised to be the optimum acidity for EC hydrogenation. In addition, the average size of Cu NPs on S-1@Cu were clearly smaller (Fig. 4d and S4), which were conducive to contact with EC. In addition, the different zeolites@Cu showed high conversion of EC, and there were great differences in the selectivities of EG and MeOH on them. This was supposed to more meteorological products in the reaction process on Beta-D@Cu and MOR-D@Cu, such as CO or CO_2. Thus, S-1@Cu was thus further studied for EC hydrogenation.

Effect of Zeolite Size

To study the effect of zeolite crystal size on the catalytic performance, the Cu NPs were loaded by abovementioned host-guest hydrothermal method on a variety of Silicalite-1 crystals that were hydrothermally synthesized by varying the chemicals or gel compositions. For all S-1-x@$CuSiO_3$ obtained from variable crystal sizes (x = 30000, 4800, 340 and 210 nm), the SEM images indicated that the needle-like phase was uniformly dispersed on the S-1 crystal surface (Fig. S5 and S6). After H_2-reduction at 250 ºC, S-1-x@Cu retained the core/shell structure (Fig. S7). When

View Article Online
DOI: 10.1039/C9GC01726G

being used for EC hydrogenation, they showed a high EC conversion (99%) except for S-1-30000@Cu (78%) (Fig. 6). However, S-1-210@Cu gave the highest MeOH selectivity, probably because of the excellent mass transfer and the optimal size of Cu particles. As shown in Table 1, the S_{ext} increased from 68 to 115 m^2 g^{-1} and V_{meso} increased from 0.26 to 0.34 cm^3 g^{-1} with decreasing S-1 crystal size from 30000 to 210 nm, favouring the diffusion of EC and MeOH molecules. Chen and co-workers reported that the Cu particles in certain size range could activate the C=O bond in EC at the step-edge sites and the variation of Cu particle size would influence the copper-silica interfacial sites, the electronic properties and Cu^0/Cu^+ species, which govern the catalytic reactivity correspondingly.[16,42] Moreover, as estimated by TEM images, the average Cu particle sizes decreased from 6.8 to 4.7 nm with decreasing S-1 size (insets in Fig. S6), which would be helpful for the contact of EC molecules with Cu particles. Considering the factors of porosity and Cu NPs size, S-1 with smaller nanocrystal like 210 nm is critical to prepare the S-1@Cu catalyst with the highest EC conversion and MeOH selectivity.

Roles of Cu^0 and Cu^+ Species on EC Hydrogenation

The co-existing Cu^0 and Cu^+ active species are the widely accepted active sites regarding of the Cu-based catalysts for the selective hydrogenation of EC. The Cu^0 species adsorb dissociated H_2 and facilitate the hydrogenation and/or hydrogenolysis reactions while the Cu^+ sites act as electrophilic or Lewis acidic sites to polarize the carbonyl groups via the electron lone pair in oxygen.[16, 17, 19-23] Nevertheless, the Cu^0/Cu^+ was greatly influenced by the reduction temperature and thus the catalytic

View Article Online
DOI: 10.1039/C9GC01726G

performance was affected correspondingly. The H_2-TPR profile on the calcined S-1-210@$CuSiO_3$ sample showed that the Cu^{2+} species started to be reduced at 115 ºC (Fig. S8). Hence, the reduction temperature from 150 to 450 ºC was examined on S-1-210@Cu to investigate the influence of surface Cu^0 and Cu^+ species. Irrespective of the reduction temperature in the range of 150 to 450 ºC, S-1-210@Cu showed a complete EC conversion (99%) and a high EG selectivity (>99%) (Fig. 7). However, the MeOH selectivity showed a volcano-like curve versus the reduction temperature. A superb MeOH selectivity (93%) was achieved when the S-1-210@Cu catalyst was reduced at 250 ºC, while the lowest one (67%) was encountered when the S-1-210@Cu catalyst was reduced at 450 ºC. Such a big change in MeOH selectivity may be caused by the different surface compositions and chemical states on S-1@Cu. Thus, *in-situ* XPS spectra was measured to determine the surface chemical states for the S-1-210@Cu samples after H_2-reduction at different temperatures. The Cu2p XPS spectra of *in-situ* reduced S-1-210@Cu show that the Cu $2p_{3/2}$ and Cu $2p_{1/2}$ peaks appear at binding energies of 933.5 and 953.8 eV with the absence of the shakeup satellite peak (Fig. 8A). This suggests that the Cu^{2+} species in S-1-210@$CuSiO_3$ precursors can be readily reduced by H_2-reduction at 150 - 450 ºC. The Cu LMM Auger spectra indicate the Cu^0/Cu^+ species co-existed in S-1-210@Cu, and their ratio varied with the reduction temperature (Fig. 8B). The peak area integration provided quantitative information about the surface $Cu^0/(Cu^0+Cu^+)$ ratios. The Cu^0 percentage increased from 52.9% to 77.4% with raising the reduction temperature from 150 to 450 ºC, that is, more Cu^0 species can be detected at higher reduction temperature.

View Article Online
DOI: 10.1039/C9GC01726G

Therefore, the highest MeOH selectivity was obtained on S-1-210@Cu with a $Cu^0/(Cu^0+Cu^+)$ ratio of 63.2%, which is presumed to be the optimum Cu^0/Cu^+ combination for selective production of MeOH.

A recent study reported that the electropositive copper species (Cu^+) strongly interacted with the surface of SiO_2 with strong Lewis acidity.[43] The acidic property of the S-1-210@Cu composites was investigated by NH_3-TPD technique (Fig. 9). The acid concentration decreased greatly from 221.9 to 31.2 $mmol \cdot g^{-1}$ with increasing reduction temperature from 150 to 450 ºC. This can be taken as an indirect evidence that high temperature is more conducive to formation of Cu^0. In order to further investigate the acidic property of the zeolites, FTIR spectra of adsorbed pyridine were measured for the S-1-210@Cu reduced at different temperature (Fig. S9). In agreement with the former observation from the NH_3-TPD curves, the amount of LAS was slightly decreased with the increase of reduction temperature from 150 to 450 ºC. Molecular CO can be adsorbed strongly onto Cu^+ to form carbonyls, which is considered to be the most appropriate probe molecule in characterizing Cu^+ sites.[44,45] Fig. S10 shows CO-adsorbed FTIR spectra of the S-1-210@Cu catalysts after reduced from 150 to 450 ºC. All four S-1-210@Cu catalysts showed a peak located at 2123 cm^{-1} which can be assigned to Cu^+-CO carbonyls after CO adsorption at 25 ºC.[46,47] The intensity of the bands at around 2123 cm^{-1} was integrated to semi quantify the relative amounts of Cu^+ in the S-1-210@Cu samples with the same Cu content but different reduction temperature. The intensity of the bands at around 2123 cm^{-1} decreased greatly with increasing reduction temperature from 150 to 450 ºC, which

View Article Online
DOI: 10.1039/C9GC01726G

showed the amount of Cu^+ decreased with increasing reduction temperature. Thus, the synergistic cooperation of the Cu sites with different valence states and optimized Cu^0/Cu^+ distributions are assumed to play a critical role for the selective EC hydrogenation to MeOH and EG.

Table S2 shows that CO_2 and CO were detected as main by-products in the hydrogenation process of EC with the MeOH balance around 97%. The side-reactions were mainly caused by the presence of trace water or H_2 in the reaction, which promoted the hydrolysis of EC to produce EG, CO_2 and CO.[17,48]

Effect of Copper Content

To demonstrate the synthetic controllability, a series of S-1-210@Cu materials were synthesized with different Cu contents. The ICP analysis showed they contained the actual Cu loadings of 13.6, 17.4, 21.4, 25.2 and 31.7 wt.%. The TEM images evidenced that the core/shell structures were well constructed after reduction in the S-1-210@Cu composites in a wide range of Cu content, and the SiO_2 nanorods in shell part were populated with increasing Cu content (Fig. 10). The ultrafine Cu NPs were well dispersed among the SiO_2 matrices and their size distribution was still centred at about 5.0 nm even at a Cu loading up to 31.7 wt.% (Fig. 10e, inset). Thus, this synthetic method can control the Cu loading in a wide range and make the monodispersed Cu NPs not aggregate.

Subsequently, the S-1-210@Cu catalysts were evaluated in the EC hydrogenation after reduction at the optimal temperature of 250 ºC. Fig. 11 presents the Cu loading-dependent EC conversion and product selectivity. All the catalysts

View Article Online
DOI: 10.1039/C9GC01726G

showed the excellent EC conversion (99%) and EG selectivity (>99%). With increasing Cu content, the MeOH selectivity first increased from 61% to 93%, reaching the maximum value at 21.4 wt.% Cu content. It then decreased to 66% with further increasing the Cu content to 31.7 wt.%. The highest MeOH selectivity afforded by S-1-210@Cu-21.4 is supposed to be related to its well-balanced mass transfer, Cu NPs size and Cu^{+}/Cu^{0} ratio. As shown in Table 1, the S_{ext} increased from 99 to 141 $m^2\ g^{-1}$ and V_{meso} increased from 0.36 to 0.52 $cm^3\ g^{-1}$ with the increase of Cu content from 13.6 to 31.7 wt.%, which would favour the diffusion of EC and MeOH molecules. The average size of Cu NPs changed slightly from 4.4 to 5.0 nm with increasing Cu loading (Fig. 10). The bigger Cu NPs were detrimental to the contact with the reactants. The deconvolution results from the Cu LMM Auger electron spectra showed that the surface $Cu^0/(Cu^0+Cu^+)$ ratios decreased from 56.8% to 69.5% with the increase of Cu contents (Fig. S11). Taking into account the optimum 63.2% $Cu^0/(Cu^0+Cu^+)$ ratio for EC hydrogenation and other two factors, S-1-210@Cu-21.4 is reasonable to exhibit the highest MeOH selectivity among the five catalysts investigated.

Effect of Solvent and $WHSV_{EC}$

Table S3 shows the batch-wise reaction results of the selective hydrogenation of EC over S-1@Cu catalysts in different solvents. It should be noted that the S-1@Cu catalyst with Cu content of 21.4 wt.% showed high EC conversion in 1, 4-dioxane (98%) and ethanol (97%) but very low conversion in gamma valerolactone (34%). Meanwhile, the S-1@Cu catalyst showed higher MeOH selectivity (74%) and EG

View Article Online
DOI: 10.1039/C9GC01726G

selectivity (99%) in 1, 4-dioxane than in ethanol with 9% MeOH selectivity and 60% EG selectivity. In terms of activity, 1,4-dioxane proved to be the most suitable solvent for the selective hydrogenation of EC on the S-1@Cu catalyst.

In order to further optimize the reaction conditions, the activities of EC hydrogenation over S-1@Cu catalyst at different $WHSV_{EC}$ were compared. Fig. 12 presented the EC conversion and product selectivity over S-1@Cu catalyst with the $WHSV_{EC}$ changing from 0.13 to 0.91. The EC conversion decreased from 99% to 81% with increasing $WHSV_{EC}$ from 0.13 to 0.91, meaning the active sites in the S-1@Cu catalyst with Cu content of 21.4 wt.% were not enough to activate hydrogen and adsorb EC at very high $WHSV_{EC}$.[49] Moreover, the MeOH selectivity decreased from 93% to 77% and MeOH selectivity decreased from 99% to 94% with the increase of $WHSV_{EC}$ from 0.13 to 0.91. Thus, the lower $WHSV_{EC}$ (0.13) is more suitable to achieve higher EC conversion and MeOH selectivity.

Stability

The stability of the optimal S-1-210@Cu-21.4 catalyst is also an important matter from the viewpoint of real application. Fig. 13 displays the long-term catalytic performance as a function of reaction time. S-1-210@Cu-21.4 exhibited not only high MeOH selectivity but also superior stability for continuous EC hydrogenation, which could be ascribed to the inclusion of SiO_2 nanorodes between Cu NPs and the presence of stable Cu^+ species. The used catalyst after 550 h running showed in XRD pattern two obvious diffractions at 2θ of 42.3º and 43.3º, attributed to Cu^0 (111) and Cu_2O (200) planes, and a new diffraction at 50.4º indexed as the Cu^0 (200) species

View Article Online
DOI: 10.1039/C9GC01726G

(Fig. 14A). This is indicative of the agglomeration/growth of Cu^0 and Cu_2O. This finding was also verified by TEM investigation. The used S-1-210@Cu-21.4 showed enlarged Cu NPs with 12 - 28 nm in diameter (Fig. S12). Furthermore, the TG analysis shows that the deposition of carbonaceous on the spent S-1-210@Cu-21.4 was observed about 2.52 % over 260 ºC (Fig. 14B). The deactivation thus is probably caused by agglomeration/growth of Cu NPs and coke deposition.

Furthermore, the reusability of the S-1-210@Cu-21.4 catalyst was also evaluated in a batch-wise reactor for hydrogenation of EC to MeOH and EG. As shown in Fig S13, the catalyst suffered obvious deactivation and showed the EC conversion of 89% and MeOH selectivity of 65% after two consecutive runs. However, the activity of the S-1-210@Cu-21.4 catalyst can be slightly recovered with the the EC conversion of 91% and MeOH selectivity of 70% after regeneration by washing with solvent followed by drying at 120 ℃ to remove the organic compounds occluded in the catalyst.

FTIR Investigation into EC Hydrogenation Mechanism

In order to clarify the reaction pathway on S-1@Cu catalyst, the evolution of the adsorbed EC molecules in N_2 or N_2/H_2 atmosphere was studied in detail by FTIR spectroscopy. The spectra of S-1-210 and S-1-210@Cu-21.4 are in good agreement with those MFI zeolite (Fig. S14), displaying the framework vibration overtones at 1632, 1882 and 2007 cm^{-1}.[50] Fig. 15a and S15a shows the FTIR spectra of the adsorbed EC on S-1-210@Cu-21.4 under N_2 atmosphere at 180 ºC. The main bands of EC at 1805 and 1772 cm^{-1} are assigned to $\nu_{C=O}$, whereas those at 1477 and 1389

View Article Online
DOI: 10.1039/C9GC01726G

cm^{-1} are attributed to δ_{CH2} and $\delta_{CH2(sc)}$.[51] The bands at 3000 and 2930 cm^{-1} are assigned to the C-H asymmetric stretching. After switching to 5% H_2/N_2, the intensities of vibrations associated with EC at 1805 and 1772 cm^{-1} decreased gradually, along with appearance of some new broad bands (Fig. 15b and S15b). The wide band in the range of 1445 to 1469 cm^{-1} could be assigned to $\delta_{CH3(as)}$ and $_{CH2}$ due to the newly formed MeOH and EG.[52,53] In addition, the new broad band at 2979 to 2946 cm^{-1} appeared in the C-H stretching vibration region, and the bands at 2887 and 2848 cm^{-1} also increased in intensity (Fig. 15c, 15d, S15c and S15d), indicating the formation of new species.[54,55] Fig. S16 shows the FTIR spectra of the adsorbed EC on Cu-free S-1-210 and unreduced S-1-210@$CuSiO_3$-21.4 after introducing 5% H_2/N_2, respectively. The IR bands associated to MeOH or EG did not appear on these samples, in contrast with the S-1-210@Cu-21.4 catalyst. The above results further proved that Cu^0 and Cu^+ species are the essential active species for the selective hydrogenation of EC to MeOH and EG.

Further Discussion

The core/shell structure S-1@Cu possessed SiO_2 shell with needle-like morphology, on which highly dispersed Cu NPs were immobilized. The immobilization process of Cu NPs induced the *in-situ* construction of mesopores, due to the base-assisted chemoselective extraction of Si species from the framework of the zeolite and thus forming the looser SiO_2 on the surface of S-1. Such mesoporous architecture endowed the S-1@Cu catalyst with large external surface area (S_{ext}) and high mesopore volumes (V_{meso}) (in Table 1), which guaranteed the maximal exposure

View Article Online
DOI: 10.1039/C9GC01726G

of Cu^0/Cu^+ active sites, as well as the improved diffusion of reactants and products molecules during the reaction process. For instance, the S_{ext} remarkably increased from 57 m^2 g^{-1} for S-1 to 117 m^2 g^{-1} for S-1@Cu-21.4, meanwhile the V_{meso} increased from 0.12 to 0.41 cm^3 g^{-1} accordingly. These physicochemical properties of the S-1@Cu catalysts with large external surface area and mesopore volumes ensured that the hydrogenation of EC over the S-1@Cu catalyst achieved relatively higher activity and selectivity.

When recalling the catalytic performance of zeolite@Cu catalysts with different zeolite topologies, crystal sizes, different Cu^0/Cu^+ ratios and different copper contents, the S-1-210@Cu-21.4 afforded the best catalytic performance for the selective hydrogenation of EC in a fixed-bed reactor. In order to better understand the catalytic behavior of the S-1-210@Cu-21.4 catalyst for the selective hydrogenation of EC to MeOH and EG, we compared the S-1-210@Cu-21.4 catalyst with the heterogeneous Cu catalysts reported in the literature and summarized the detailed results in Table S4. In terms of catalytic performance, the conversion of EC and selectivity to EG showed no significant difference for all the Cu-based catalysts. However, the selectivity to MeOH was quite different. For instance, the 50Cu/HMS catalyst with the Cu content of 44.6 wt.% exhibited a 74% selectivity to MeOH at 180 ºC under 3MPa of H_2. [17] The 0.7Cu/MCM-41 catalyst gave 70.0% and 98% selectivity to MeOH and EG, respectively, at 180 ºC under 3 MPa of H_2.[49] The 70%Cu-SiO_2-PG catalyst with a 56 wt.% copper content under the hydrogen pressure of 6.0 MPa furnished the highest MeOH selectivity of 97%, the highest selectivity for the EC hydrogenation to MeOH

View Article Online
DOI: 10.1039/C9GC01726G

reported up to now.[16] With regards of the home-made S-1@Cu catalyst, it afforded >93% selectivity to MeOH under 4.0 MPa of H_2 with a Cu loading of 21.4 wt.%, which is lower than a half of that in 70%Cu-SiO_2-PG. Moreover, the hydrogen pressure of 4.0 MPa for the S-1@Cu catalyst giving >93% selectivity to MeOH is also much lower in comparison with 6.0 MPa for the 70%Cu-SiO_2-PG catalyst furnishing a 97% selectivity to MeOH. In our previous research, we found that the selectivity to MeOH increased remarkably with the increase of hydrogen pressure.[18] Additionally, the stability of the S-1@Cu catalyst is also the most excellent among all of the C-based catalysts. As also listed in Table S4, the 70%Cu-SiO_2-PG catalyst showed a lifetime of about 80 h, while the 50Cu/HMS showed a lifetime over 100 h. The deactivation of 0.7Cu/MCM-41 occurred within 100 h and the activity on Cu-Mg-Zr/SiO_2 could be maintained for 100 h without any deactivation. Compared with these Cu catalysts reported in the literatures, the S-1@Cu catalyst in this work exhibited high performance within 350 h. Even after 350 h, the selectivity to MeOH only slightly declined and about 80% selectivity to MeOH was still afforded by the S-1@Cu catalyst after 500 h, which is even higher than the fresh Cu catalysts in some cases (Table S4, entries 1, 3, 4, 5 and 6).

Conclusions

In summary, we have developed a novel route for preparing a well-dispersed Cu^0/Cu^+ species supported on Silicalite-1 zeolite through the reduction of core/shell S-1@$CuSiO_3$, in which the $CuSiO_3$ phase was vertically grown on the S-1 crystal via a base-assisted hydrothermal chemistry. This method realizes the in-situ construction

View Article Online
DOI: 10.1039/C9GC01726G

of mesopores and high dispersion of Cu NPs, simultaneously. With a suitable Cu^0/Cu^+ ratio, the prepared S-1@Cu composite serves as an efficient and stable EC hydrogenation catalyst, exhibiting a superior MeOH selectivity (93%) and EG selectivity (>99%) at a relatively low copper content of 21.4 wt.%.

Conflict of interest

There are no conflicts to declare.

Acknowledgments

The authors gratefully acknowledge the financial support from National Natural Science Foundation of China (Grant Nos.21872052, 21533002 and 21571128), China Ministry of Science and Technology (2016YFA0202804).

References

1 S. Solomon, G. K. Plattner, R. Knutti, P. Friedlingstein, *Proc. Natl. Acad. Sci. U. S. A.*, 2009, **106**, 1704-1709.

2 P. Markewitz, W. Kuckshinrichs, W. Leitner, J. Linssen, P. Zapp, R. Bongartz, A. Schreiber, T. E. Muller, *Energy Environ. Sci.*, 2012, **5**, 7281-7305.

3 M. Pérez-Fortes, J. C. Schöneberger, A. Boulamanti, E. Tzimas, *Appl. Energy*, 2016, **161**, 718-732.

4 M. Bukhtiyarova, T. Lunkenbein, K. Kähler, R. Schlögl, *Catal. Lett.*, 2017, **147**, 416-427.

5 A. Goeppert, M. Czaun, J. Jones, G. K. Surya Prakash, G. A. Olah, *Chem. Soc. Rev.*, 2014, **43**, 7995-8048.

6 M.Aresta, A. Dibenedetto, A. Angelini, *Chem. Rev.*, 2014, **114**, 1709-1742.

7 A. Bansode, A. Urakawa, *J. Catal.*, 2014, **309**, 66-70.

8 W. Wang, S. P. Wang, X. B. Ma, J. L. Gong, *Chem. Soc. Rev.*, 2011, **40**,

View Article Online
DOI: 10.1039/C9GC01726G

3703-3727.

9 P. Gao, F. Li, H. J. Zhan, N. F. Zhao, K. Xiao, W. Wei, L. S. Zhong, Y. H. Sun, *Catal. Commun.*, 2014, **50**, 78-82.

10 T. Sakakura, J. C. Choi, H. Yasuda, *Chem. Rev.*, 2007, **107**, 2365-2387.

11 E. Balaraman, C. Gunanathan, J. Zhang, L. J. W. Shimon, D. Milstein, *Nat. Chem.*, 2011, **3**, 609-614.

12 Z. Han, L. Rong, J. Wu, L. Zhang, Z. Wang, K. Ding, *Angew. Chem. Int. Ed.*, 2012, **51**, 13041-13045.

13 X. Lu, R. He, C-X. Bai, *J. Mol. Catal. A*, 2002, **186**, 1-11.

14 L. T. Omae, *Coord. Chem. Rev.*, 2012, **256**, 1384-1405.

15 C. Lian, F. M. Ren, Y. X. Liu, G. F. Zhao, Y. J. Ji, H. P. Rong, W. Jia, L. Ma, H. Y. Lu, D. S. Wang, Y. D. Li, *Chem. Commun.*, 2015, **51**, 1252-1254.

16 H. L. Liu, Z. W. Huang, Z. B. Han, K. L. Ding, H. C. Liu, C. G. Xia, J. Chen, *Green Chem.*, 2015, **17**, 4281-4290.

17 X. Chen, Y. Cui, C. Wen, B. Wang, W-L. Dai, *Chem. Commun.*, 2015, **51**, 13776-13778.

18 J. Tian, W. Chen, P. Wu, Z. Zhu, X. Li, *Catal. Sci. Technol.*, 2018, **8**, 2624-2635.

19 A. Yin, X. Guo, W. L. Dai, K. Fan, *J. Phys. Chem. C*, 2009, **113**, 11003-11013.

20 Y. Zhu, X. Kong, S. Zhu, F. Dong, H. Zheng, Y. Zhu, Y. W. Li, *Appl. Catal., B*, 2015, **166**, 551-559.

21 Y. Wang, Y. Shen, Y. Zhao, J. Lv, S. Wang, X. Ma, *ACS Catal.*, 2015, **5**, 6200-6208.

22 C. Zhang, L. Wang, J. Liu, Y. Yang, P. He, Y. Cao, J. Chen, H. Li, *ChemCatChem*, 2018, **10**, 4617-4628.

23 Z. Wang, Z. Xu, S. Peng, M. Zhang, G. Lu, Q. Chen, Y. Chen, G. Guo, *ACS Catal.*,

View Article Online
DOI: 10.1039/C9GC01726G

2015, **5**, 4255-4259.

24 Z. Zhu, H. Xu, J. Jiang, H. Wu, P. Wu, *ACS Appl. Mater. Interfaces*, 2017, **9**, 27273-27283.

25 L. Wu, L. Li, B. Li, C. Zhao, *Chem. Commun.*, 2017, **53**, 6152-6155.

26 H. Peng, L. Xu, H. Wu, Z. Wang, Y. Liu, X. Li, M. He, P. Wu, *Microporous Mesoporous Mater.*, 2012, **153**, 8-17.

27 J. Gong, H. Yue, Y. Zhao, S. Zhao, L. Zhao, J. Lv, S. Wang, X. Ma, *J. Am. Chem. Soc.*, 2012, **134**, 13922-13925.

28 T. Toupance, M. Kermmarec, J. F. Lambert, C. Louis, *J. Phys. Chem. B*, 2002, **106**, 2277-2286.

29 Z. Huang, F. Cui, H. Kang, J. Chen, X. Zhang, C. Xia, *Chem. Mater.*, 2008, **20**, 5090-5099.

30 Z. He, H. Q. Lin, P. He, Y. Z. Yuan, *J. Catal.*, 2011, **277**, 54-63.

31 F. Li, L. Wang, X. Han, Y. Cao, P. He, H. Li, *Int. J. Hydrogen Energy,* 2017, **42**, 2144-2156.

32 J. Tian, J. Hu, W. Shan, P. Wu, X. Li, *Appl. Catal. A*, 2017, **544**, 108-115.

33 X. Huang, M. Ma, S. Miao, Y. Zheng, M. Chen, W. Shen, *Appl. Catal. A,* 2017, **531**, 79-88.

34 Z. Lu, H. Yin, A. Wang, J. Hu, W. Xue, H. Yin, S. Liu, *J. Ind. Eng. Chem.,* 2016, **37**, 208-215.

35 T. Ghodselahi, M. A. Vesaghi, A. Shafiekhani, A. Baghizadeh, M. Lameii, *Appl. Surf. Sci.*, 2008, **255**, 2730-2734.

36 M. Biesinger, L. Lau, A. Gerson, R. Smart, *Appl. Surf. Sci*., 2010, **257,** 887-898.

37 Y. Cui, W-L. Dai, *Catal. Sci. Technol*., 2016, **6**, 7752-7762.

38 D. J. Thomas, J. T. Wehrli, M. S. Wainwright, D. L. Trimm, N. W. Cant, *Appl.*

View Article Online
DOI: 10.1039/C9GC01726G

Catal. A, 1992, **86**, 101-114.

39 M. A. N. Santiago, M. A. Sanchez-Castillo, R. D. Cortright, J. A. Dumesic, *J. Catal.*, 2000, **193**, 16-28.

40 L. F. Chen, P. J. Guo, M. H. Qiao, S. R. Yan, H. X. Li, W. Shen, H. L. Xu, K. N. Fan, *J. Catal.*, 2008, **257**, 172-180.

41 E. P. Parry, *J. Catal*., 1963, **2**, 371-379.

42 R. A. Van Santen, *Acc. Chem. Res.*, 2009, **42**, 57-66.

43 Y. Zhu, Y. Zhu, G. Ding, S. Zhu, H. Zheng, Y. Li, *Appl. Catal. A*, 2013, **468**, 296-304.

44 K. Hadjiivanov, L. Dimitrov, *Micropor. Mesopor. Mater.*, 1999, **27**, 49–56.

45 J. Xue, X. Wang, G. Qi, J. Wang, M. Shen, W. Li, *J. Catal.*, 2013, **297**, 56-64.

46 H. Wan, Z. Wang, J. Zhu, X.W. Li, B. Liu, F. Gao, L. Dong, Y. Chen, *Appl. Catal., B*, 2008, **79**, 254–261.

47 T. Tsoncheva, T. Venkov, M. Dimitrov, C. Minchev, K. Hadjiivanov, *J. Mol. Catal. A: Chem.*, 2004, **209**, 125-134.

48 Y. Li, K. Junge, M. Beller, *ChemCatChem*, 2013, **5**, 1072-1074.

49 F. Deng, N. Li, S. Tang, C. Liu, H. Yue, B. Liang, *Chem. Eng. J*., 2018, **334**, 1943-1953.

50 J. A. Zhou, Z. L. Hua, Z. C. Liu, W. Wu, Y. Zhu, J. L. Shi, *ACS Catal.*, 2011, **1**, 287-291.

51 Y. Ikezawa, H. Nishi, *Electrochimica Acta*, 2008, **53**, 3663-3669.

52 G. J. Millar, C. H. Rochester, K. C. Waugh, *J. Chem. Soc. Faraday Trans.*, 1991, **87**, 2795-2804.

53 I. A.Fisher, A. T. Bell, *J. Catal.*, 1999, **184**, 357-376.

54 R. Srivastava, D. Srinivas, P. Ratnasamy, *J. Catal.*, 2005, **233**, 1-15.

View Article Online
DOI: 10.1039/C9GC01726G

55 L. Dreesen, C. Humbert, P. Hollander, A. Mani, K. Ataka, P. Thiry, A. Peremans, *Chem. Phys. Lett.*, 2001, **333**, 327-331.

View Article Online
DOI: 10.1039/C9GC01726G

Figure Captions

Fig. 1 High resolution XRD patterns of S-1 (a), S-1@$CuSiO_3$ (b) and S-1@Cu (c).

Fig. 2 IR spectra of S-1 (a), S-1@$CuSiO_3$ (b) and S-1@Cu (c).

Fig. 3 (A) The in-situ Cu 2p spectra of S-1@$CuSiO_3$ (a) and S-1@Cu (b), (B) Cu LMM Auger electron spectra of the S-1@Cu catalyst.

Fig. 4 TEM images of S-1@$CuSiO_3$ (a and b) and S-1@Cu (d and e) with 21.4 wt.% Cu loading. SEM images of S-1@$CuSiO_3$ (c) and S-1@Cu (f) with 21.4 wt.% Cu loading. The inset shows the Cu NPs size distribution in Fig. 4d.

Fig. 5 N_2 adsorption-desorption isotherms at 77 K of S-1 (a) and S-1@Cu (b).

Fig. 6 Conversion of EC and selectivity to MeOH and EG over the S-1@Cu catalysts with similar copper content of 22 wt.% and different particle sizes. Reduction condition: 250 ºC, 4 h, H_2 (60 mL min^{-1}); reaction conditions: 1g S-1-210-x@Cu (x = 30000, 4800, 340 and 210 nm), 180 ºC, 4 h, 4 MPa H_2, $GHSV_{H2}$ = 2400, $WHSV_{EC}$ = 0.13.

Fig. 7 Conversion of EC and selectivity to MeOH and EG as a function of reduction temperature of S-1-210@Cu-21.4. Reduction condition: 4 h, H_2 (60 mL min^{-1}); reaction conditions: 1g S-1-210@Cu-21.4, 180 ºC, 4h, 4 MPa H_2, $GHSV_{H2}$ = 2400, $WHSV_{EC}$ = 0.13.

Fig. 8 In-situ Cu 2p XPS spectra (A) and Cu LMM Auger electron spectra (B) of the S-1-210@Cu catalysts prepared after H_2-reduction at 150 ºC (a), 250 ºC (b), 350 ºC (c) and 450 ºC (d).

Fig. 9 NH_3-TPD profiles of the S-1-210@Cu catalysts prepared by H_2-reduction at

View Article Online
DOI: 10.1039/C9GC01726G

150 ºC (a), 250 ºC (b), 350 ºC (c) and 450 ºC (d).

Fig. 10 TEM images of S-1-210@Cu-13.6 (a), S-1-210@Cu-17.4 (b), S-1-210@Cu-21.4 (c), S-1-210@Cu-25.2 (d) and S-1-210@Cu-31.7 (e) reduced at 250 ºC. The insets show the distribution of Cu NPs sizes.

Fig. 11 Conversion of EC hydrogenation and selectivity to MeOH and EG as a function of the Cu content of S-1-210@Cu. Reaction conditions: S-1-210@Cu, 1 g; temp., 180 ºC; time, 4 h; H_2 pressure, 4 MPa; $GHSV_{H2}$=2400; $WHSV_{EC}$ = 0.13. Reduction: 250 ºC; 4 h; H_2 (60 mL min^{-1}).

Fig. 12 Conversion of EC hydrogenation and selectivity to MeOH and EG as a function of the $WHSV_{EC}$. Reaction conditions: S-1-210@Cu, 1 g; temp., 180 ºC; time, 4 h; H_2 pressure, 4 MPa; $GHSV_{H2}$=2400. Reduction: 250 ºC; 4 h; H_2 (60 mL min^{-1}).

Fig. 13 Long-term selective hydrogenation of EC to MeOH and EG over S-1-210@Cu-21.4. Reaction conditions: S-1-210@Cu-21.4, 1 g; temp., 180 ºC; H_2 pressure, 4 MPa; $GHSV_{H2}$=2400; $WHSV_{EC}$ = 0.13. Reduction: 250 ºC; 4 h; H_2 (60 mL min^{-1}).

Fig. 14 The XRD patterns (A) and TG analyses (B) of fresh S-1-210@Cu-21.4 (a) and used S-1-210@Cu-21.4 in EC hydrogenation for 550 h (b).

Fig. 15 FTIR spectra of EC (a), EG (c) and MeOH (d) absorbed on S-1-210@Cu-21.4 under N_2 atmosphere at 180 ºC. The spectrum for in-situ EC hydrogenation at 180 ºC on S-1-210@Cu-21.4 under 5% H_2/N_2 atmosphere (b).

View Article Online
DOI: 10.1039/C9GC01726G

Table 1. Physicochemical properties of S-1 and S-1@Cu samples.

No.	Sample	SSA[a] ($m^2 g^{-1}$)	S_{ext}[b] ($m^2 g^{-1}$)	V_{total}[c] ($cm^3 g^{-1}$)	V_{micro}[b] ($cm^3 g^{-1}$)	V_{meso}[d] ($cm^3 g^{-1}$)
1	S-1-210	364	57	0.31	0.19	0.12
2	S-1-210@Cu-21.4	335	117	0.52	0.11	0.41
3	S-1-30000@Cu-21.3	274	68	0.26	0.1	0.16
4	S-1-4800@Cu-22.1	287	78	0.27	0.1	0.17
5	S-1-340@Cu-21.6	328	105	0.42	0.11	0.31
6	S-1-210@Cu-13.6	363	99	0.49	0.13	0.36
7	S-1-210@Cu-17.4	344	106	0.50	0.12	0.38
8	S-1-210@Cu-25.2	337	122	0.54	0.09	0.45
9	S-1-210@Cu-31.7	341	141	0.62	0.10	0.52

[a] Specific surface area (SSA) calculated by BET method.

[b] Obtained by *t*-plot method.

[c] Pore volume measured at $P/P_0 = 0.99$.

[d] $V_{meso} = V_{tot} - V_{micro}$.

Scheme 1. The preparation of selective EC hydrogenation catalyst S-1@Cu with a core/shell structure and highly dispersed and stable Cu^0/Cu^+ NPs.

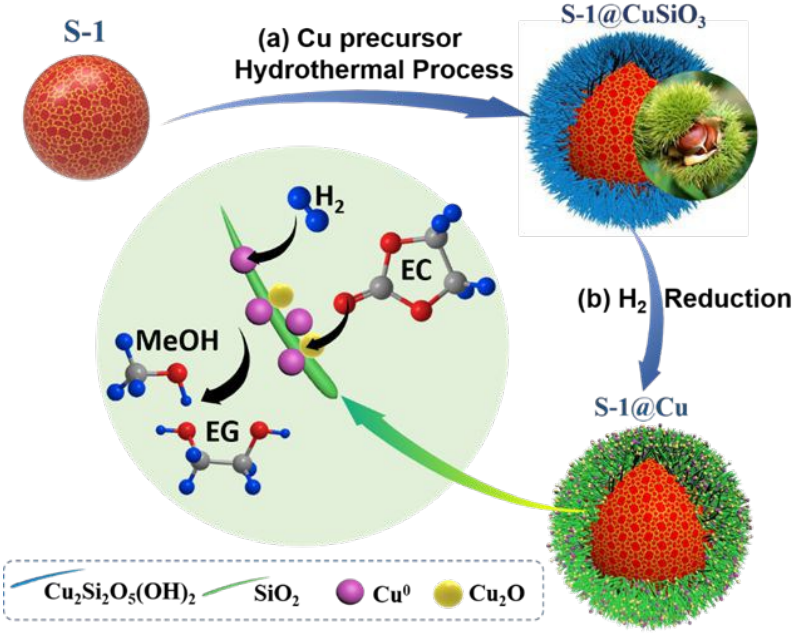

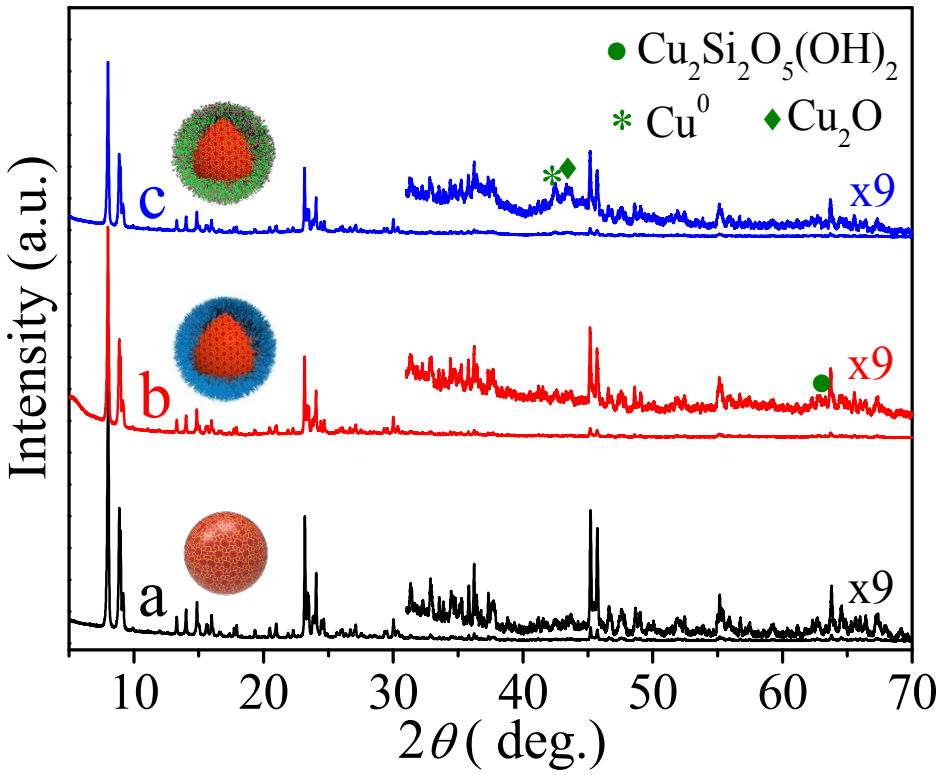

Fig. 1 High resolution XRD patterns of S-1 (a), S-1@$CuSiO_3$ (b) and S-1@Cu (c).

View Article Online
DOI: 10.1039/C9GC01726G

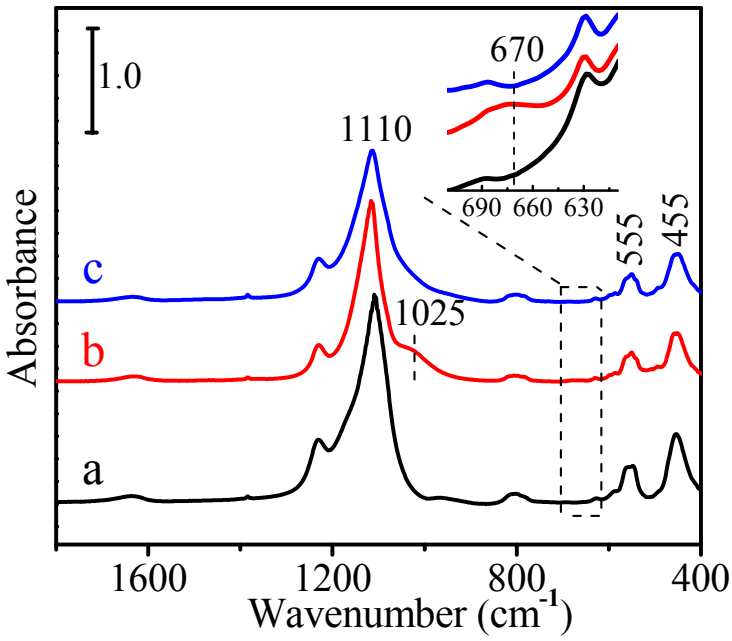

Fig. 2 IR spectra of S-1 (a), S-1@$CuSiO_3$ (b) and S-1@Cu (c).

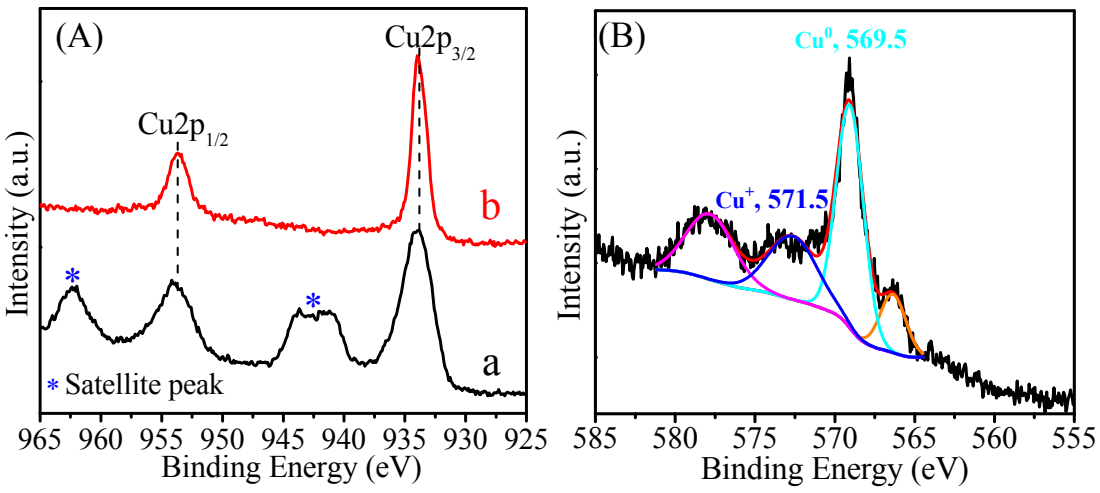

Fig. 3 (A) The in-situ Cu 2p spectra of S-1@$CuSiO_3$ (a) and S-1@Cu (b), (B) Cu LMM Auger electron spectra of the S-1@Cu catalyst.

View Article Online
DOI: 10.1039/C9GC01726G

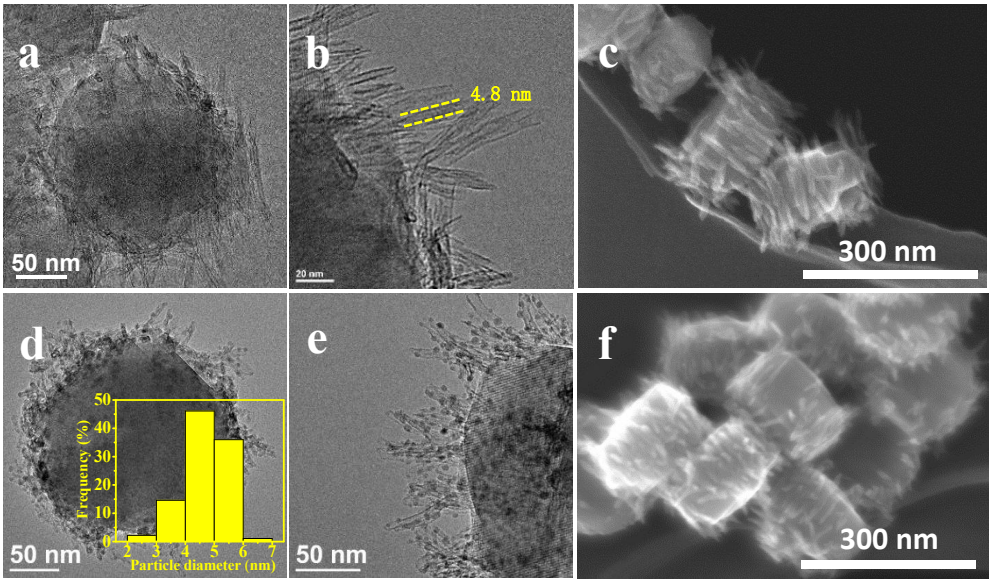

Fig. 4 TEM images of S-1@$CuSiO_3$ (a and b) and S-1@Cu (d and e) with 21.4 wt.% Cu loading. SEM images of S-1@$CuSiO_3$ (c) and S-1@Cu (f) with 21.4 wt.% Cu loading. The inset in Fig. 4d shows the Cu NPs size distribution.

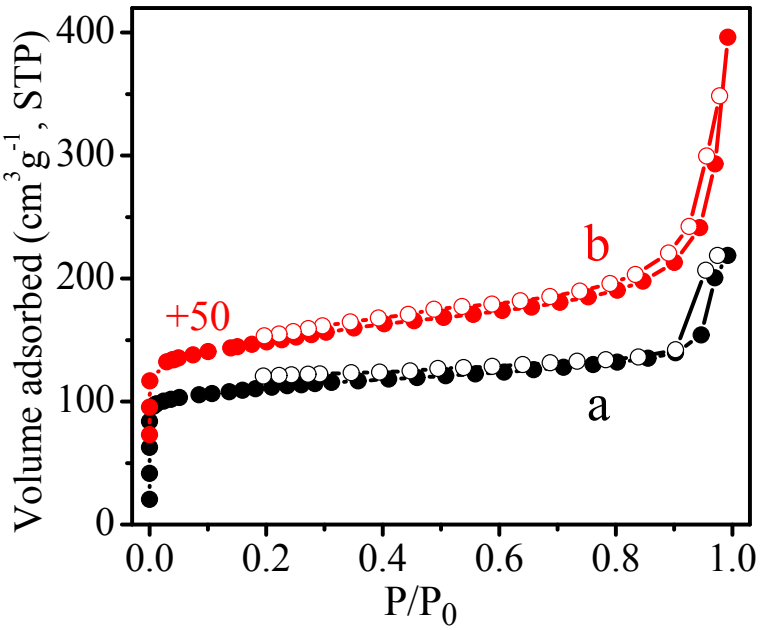

Fig. 5 N_2 adsorption-desorption isotherms at 77 K of S-1 (a) and S-1@Cu (b).

View Article Online
DOI: 10.1039/C9GC01726G

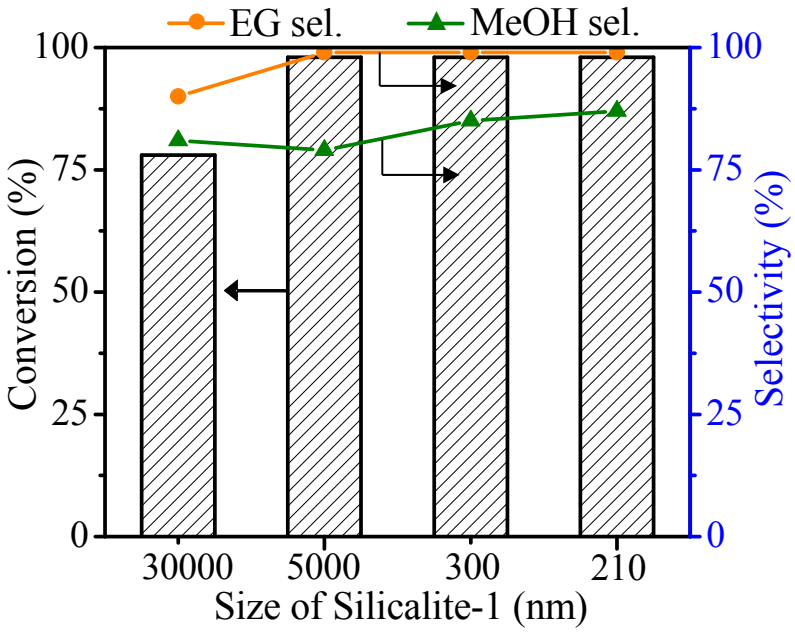

Fig. 6 Conversion of EC and selectivity to MeOH and EG over the S-1@Cu catalysts with similar copper content of 22 wt.% and different particle sizes. Reduction condition: 250 ºC, 4 h, H_2 (60 mL min^{-1}); reaction conditions: 1g S-1-210-x@Cu (x = 30000, 4800, 340 and 210 nm), 180 ºC, 4 h, 4 MPa H_2, $GHSV_{H2}$ = 2400, $WHSV_{EC}$ = 0.13.

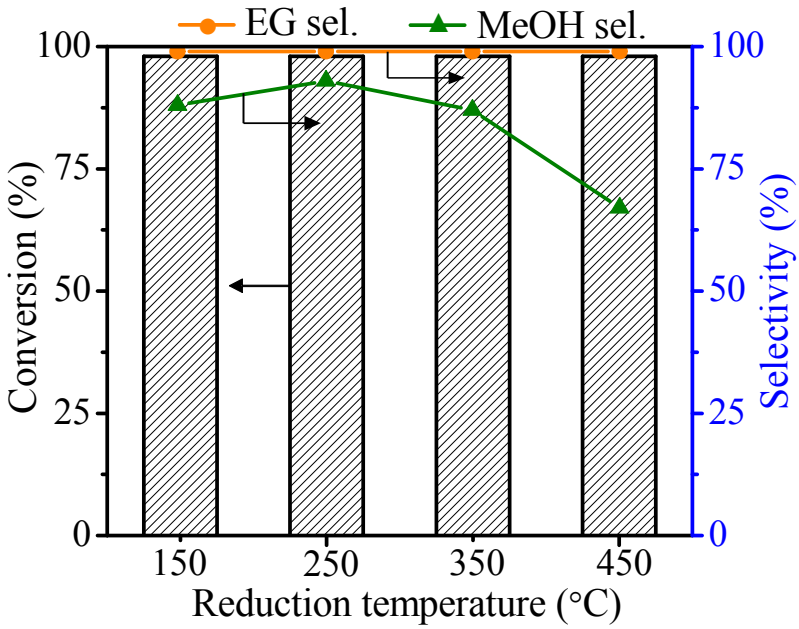

Fig. 7 Conversion of EC and selectivity to MeOH and EG as a function of reduction temperature of S-1-210@Cu-21.4. Reduction condition: 4 h, H_2 (60 mL min^{-1}); reaction conditions: 1g S-1-210@Cu-21.4, 180 ºC, 4h, 4 MPa H_2, $GHSV_{H2}$ = 2400, $WHSV_{EC}$ = 0.13.

View Article Online
DOI: 10.1039/C9GC01726G

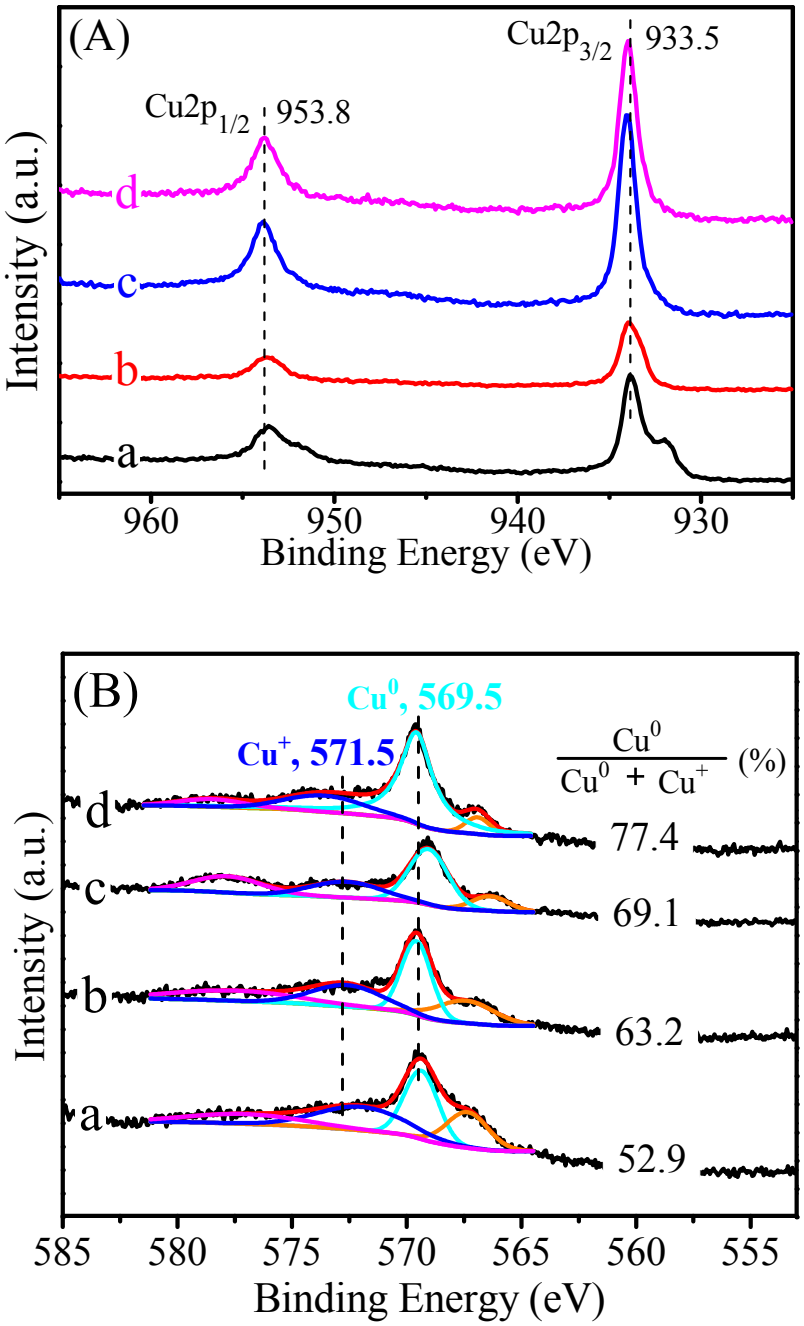

Fig. 8 In-situ Cu 2p XPS spectra (A) and Cu LMM Auger electron spectra (B) of the S-1-210@Cu catalysts prepared after H_2-reduction at 150 ºC (a), 250 ºC (b), 350 ºC (c) and 450 ºC (d).

View Article Online
DOI: 10.1039/C9GC01726G

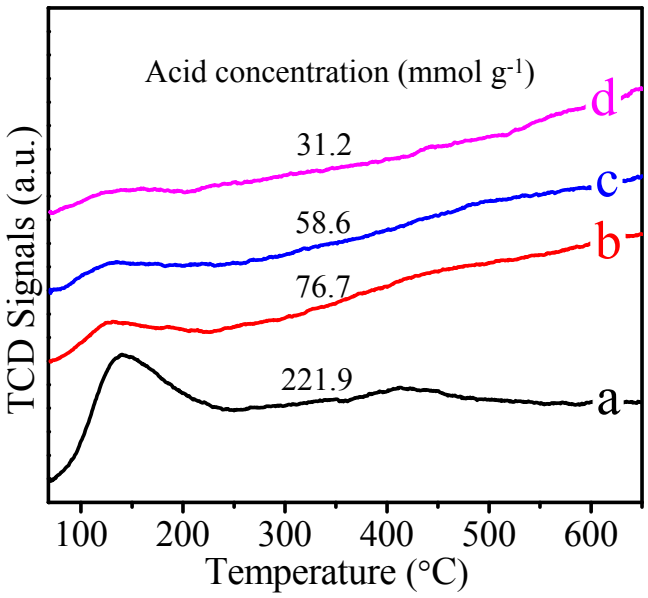

Fig. 9 NH_3-TPD profiles of the S-1-210@Cu catalysts prepared by H_2-reduction at 150 ºC (a), 250 ºC (b), 350 ºC (c) and 450 ºC (d).

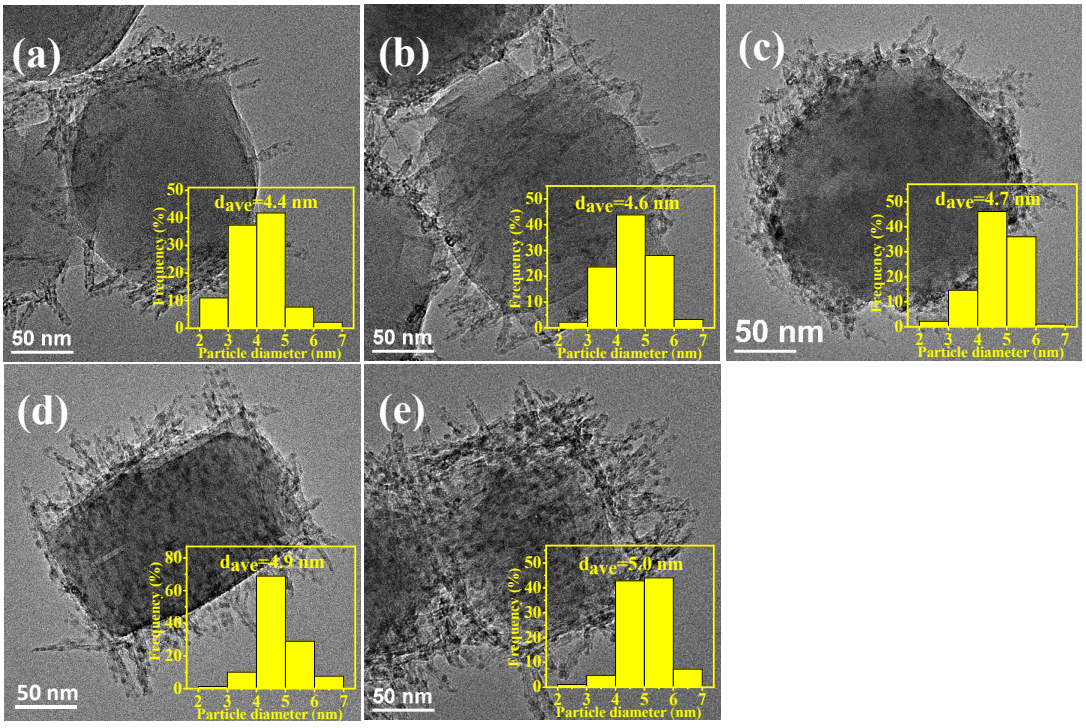

Fig. 10 TEM images of S-1-210@Cu-13.6 (a), S-1-210@Cu-17.4 (b), S-1-210@Cu-21.4 (c), S-1-210@Cu-25.2 (d) and S-1-210@Cu-31.7 (e) reduced at 250 ºC. The insets show the distribution of Cu NPs sizes.

View Article Online
DOI: 10.1039/C9GC01726G

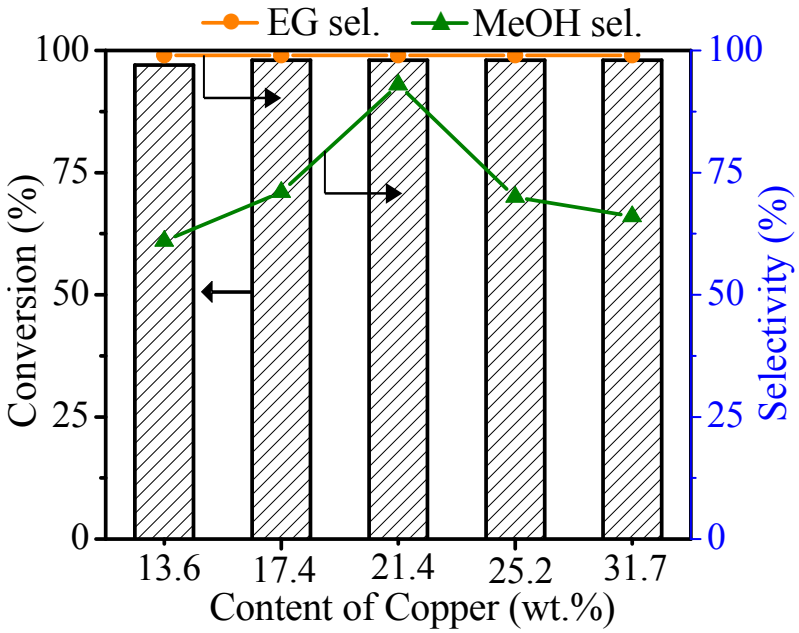

Fig. 11 Conversion of EC and selectivity to MeOH and EG as a function of the Cu content of S-1-210@Cu. Reaction conditions: S-1-210@Cu, 1 g; temp., 180 ºC; time, 4 h; H_2 pressure, 4 MPa; $GHSV_{H2}$=2400; $WHSV_{EC}$ = 0.13. Reduction: 250 ºC; 4 h; H_2 (60 mL min^{-1}).

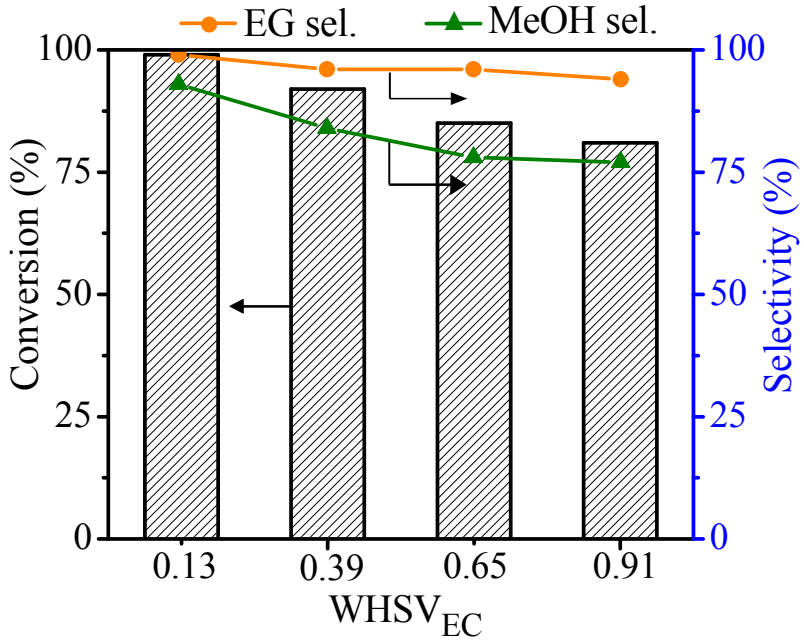

Fig. 12 Conversion of EC and selectivity to MeOH and EG as a function of the $WHSV_{EC}$. Reaction conditions: S-1-210@Cu, 1 g; temp., 180 ºC; time, 4 h; H_2 pressure, 4 MPa; $GHSV_{H2}$=2400. Reduction: 250 ºC; 4 h; H_2 (60 mL min^{-1}).

View Article Online
DOI: 10.1039/C9GC01726G

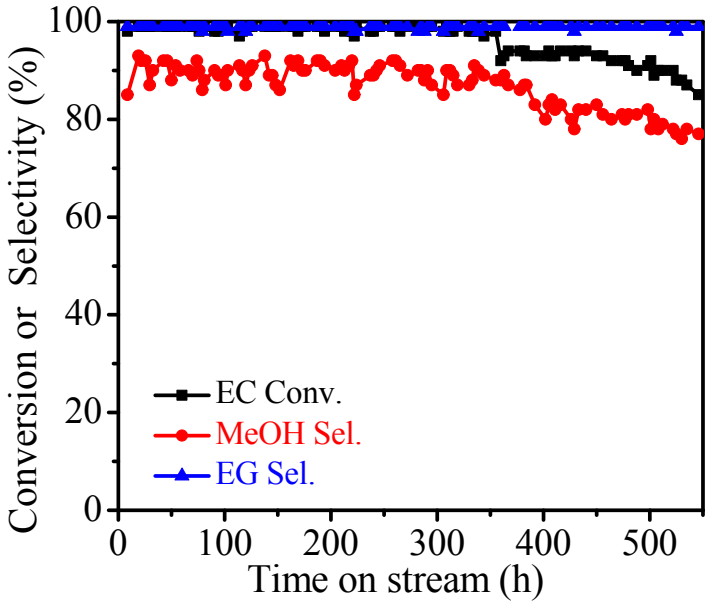

Fig. 13 Long-term selective hydrogenation of EC to MeOH and EG over S-1-210@Cu-21.4. Reaction conditions: S-1-210@Cu-21.4, 1 g; temp., 180 ℃; H_2 pressure, 4 MPa; $GHSV_{H2}$=2400; $WHSV_{EC}$ = 0.13. Reduction: 250 ℃; 4 h; H_2 (60 mL min^{-1}).

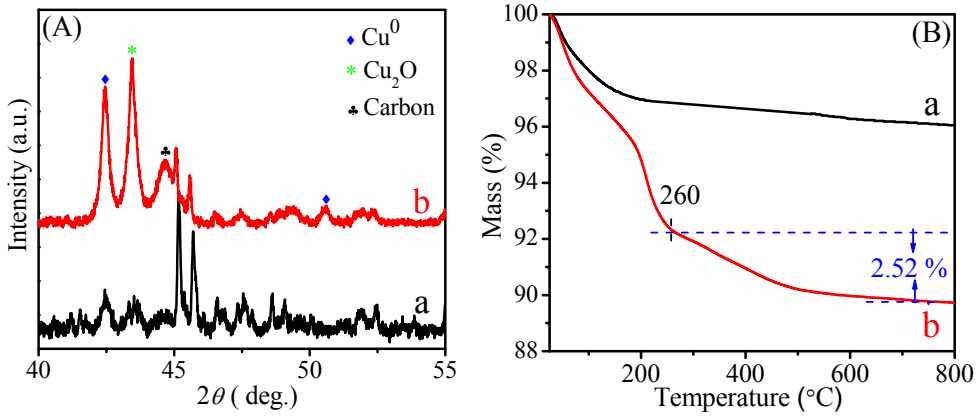

Fig. 14 The XRD patterns (A) and TG analyses (B) of fresh S-1-210@Cu-21.4 (a) and used S-1-210@Cu-21.4 in EC hydrogenation for 550 h (b).

View Article Online
DOI: 10.1039/C9GC01726G

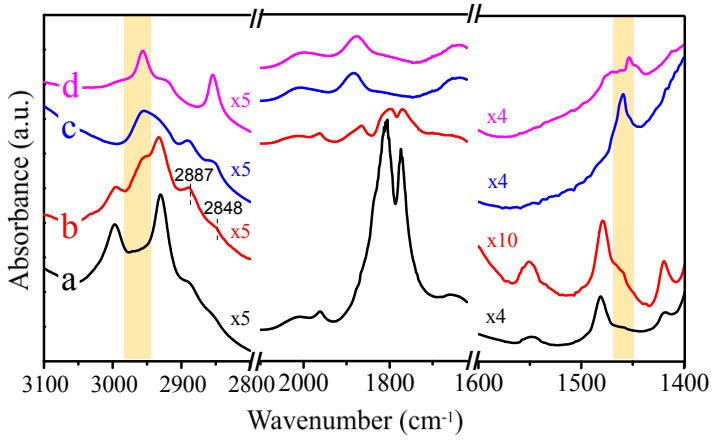

Fig. 15 FTIR spectra of EC (a), EG (c) and MeOH (d) absorbed on S-1-210@Cu-21.4 under N_2 atmosphere at 180 ºC. The spectrum for in-situ EC hydrogenation at 180 ºC on S-1-210@Cu-21.4 under 5% H_2/N_2 atmosphere (b).

View Article Online
DOI: 10.1039/C9GC01726G

Graphical Abstract

A novel hierarchical core/shell structured S-1@Cu with balanced Cu^0 and Cu^+ active species was synthesized via a base-assisted hydrothermal chemistry and served as robust catalyst for selective EC hydrogenation to methanol.